A handcuff model for the cohesin complex

Nenggang Zhang,[1] Sergey G. Kuznetsov,[2] Shyam K. Sharan,[2] Kaiyi Li,[1] Pulivarthi H. Rao,[1] and Debananda Pati[1]

[1]Department of Pediatric Hematology/Oncology, Texas Children's Cancer Center, Baylor College of Medicine, Houston, TX 77030
[2]Mouse Cancer Genetics Program, Center for Cancer Research, National Cancer Institute at Frederick, Frederick, MD 21702

The cohesin complex is responsible for the accurate separation of sister chromatids into two daughter cells. Several models for the cohesin complex have been proposed, but the one-ring embrace model currently predominates the field. However, the static configuration of the embrace model is not flexible enough for cohesins to perform their functions during DNA replication, transcription, and DNA repair. We used coimmunoprecipitation, a protein fragment complement assay, and a yeast two-hybrid assay to analyze the protein–protein interactions among cohesin subunits. The results show that three of the four human cohesin core subunits (Smc1, Smc3, and Rad21) interact with themselves in an Scc3 (SA1/SA2)-dependent manner. These data support a two-ring handcuff model for the cohesin complex, which is flexible enough to establish and maintain sister chromatid cohesion as well as ensure the fidelity of chromosome segregation in higher eukaryotes.

Introduction

An evolutionarily conserved protein complex called cohesin is responsible for the accurate separation of sister chromatids into two daughter cells. The cohesin complex comprises four core protein subunits that are conserved from yeast to vertebrates (Guacci et al., 1997; Michaelis et al., 1997; Darwiche et al., 1999). In *Saccharomyces cerevisiae* mitotic cells, the cohesin complex consists of Scc1/Mcd1 (Rad21 in humans), Smc1, Smc3, and Scc3 (Guacci et al., 1997; Michaelis et al., 1997). In human mitotic cells, the cohesin complex is composed of Rad21, Smc1α, Smc3, and two Scc3 orthologues, SA1 and SA2 (Losada et al., 2000; Sumara et al., 2000).

Smc1 and Smc3 are ABC-like ATPases. The amino terminus (NT) and carboxyl terminus (CT) of the Smc molecules fold back on themselves, forming antiparallel intramolecular coiled coils (Haering et al., 2002). The NT and CT sequences form an ABC-type ATPase domain at one end, whereas the central region becomes the hinge domain of the other end of the coiled coil. Smc1 and Smc3 form a V-shaped heterodimer via the hinge domain. The data from budding yeast show that the CT and NT of Scc1/Mcd1/Rad21 bind to the ATPase heads of the Smc1 and Smc3 heterodimer, respectively, to form a triangular ring, and Scc3 binds to Scc1/Mcd1/Rad21 to reinforce the ring (Gruber et al., 2003). The binding of ATP to the ATPase head of Smc1 is required for Scc1/Mcd1/Rad21 association with the Smc1 and Smc3 heterodimer (Arumugam et al., 2003).

Various models for sister chromatid cohesion have been proposed (Anderson et al., 2002; Campbell and Cohen-Fix, 2002; Haering and Nasmyth, 2003; Milutinovich and Koshland, 2003; Stead et al., 2003; Huang et al., 2005; Ivanov and Nasmyth, 2005; Losada and Hirano, 2005; Nasmyth, 2005; Skibbens, 2005; Guacci, 2007; Skibbens et al., 2007). Those models can be classified into three categories: one ring, two ring, and bracelet. The most frequently cited one-ring embrace model predicts that Smc1, Smc3, and Scc1/Mcd1/Rad21 form a triangular ring. Sister chromatid cohesion is established when the replication fork passes through cohesin rings (Gruber et al., 2003; Haering and Nasmyth, 2003; Nasmyth, 2005). The two-ring model proposes that each Smc heterodimer embraces one of the sister chromatids; cohesion is established when Scc1/Mcd1/Rad21 tethers the two Smc heterodimers so that two cohesin rings become paired during DNA replication (Campbell and Cohen-Fix, 2002; Stead et al., 2003; Huang et al., 2005; Nasmyth, 2005; Skibbens, 2005; Guacci, 2007; Skibbens et al., 2007). The bracelet model suggests that Scc1/Mcd1/Rad21 molecules connect Smc heterodimers, forming multimeric filaments that entrap sister chromatids (Huang et al., 2005; Nasmyth, 2005). Support for the two-ring model comes indirectly from the studies in budding yeast. Chang et al. (2005) suggest that each cohesin ring only embraces one instead of two sister chromatids in the heterochromatin regions (Huang and Moazed, 2006). A recent study shows that

Correspondence to Debananda Pati: pati@bcm.tmc.edu

Abbreviations used in this paper: CT, carboxyl terminus; CT-L, CT long; FRET, fluorescence resonance energy transfer; IP, immunoprecipitation; NT, amino terminus; NT-L, NT long; PCA, protein complement assay; WB, Western blot.

The Rockefeller University Press $30.00
J. Cell Biol. Vol. 183 No. 6 1019–1031
www.jcb.org/cgi/doi/10.1083/jcb.200801157

a pericentric chromatin organizes into a cruciform during mitosis such that the centromere-flanking DNA adopts an intramolecular loop, whereas sister chromatid arms are paired intermolecularly, suggesting a two-ring cohesin complex (Yeh et al., 2008). Although the aforementioned findings may suggest a loci- and silencing-specific mechanism that may not reflect cohesion along the length of the chromosome, they nonetheless challenge the current single-ring model, providing further indication that chromosomal cohesion is more complex than originally thought and requires additional investigation.

To understand how sister chromatids are held by cohesin complexes in higher eukaryotes, we have investigated the protein–protein interactions among the cohesin subunits in human cell lines using various biochemical and functional analyses. Our results indicate that three of the four core cohesin subunits (Rad21, Smc1, and Smc3) can coimmunoprecipitate themselves and each other, whereas the two Scc3 orthologues, SA1 and SA2, cannot. These findings suggest that a cohesin complex is not one ring. Based on the molecular associations of cohesin subunits, the results of a fluorescence protein complement assay (PCA), protein–protein interaction from a yeast two-hybrid assay, and the inhibition of SA1 and SA2 using siRNA, we provide evidence for a handcuff model of the cohesin complex, which consists of two rings. Each ring has one set of Rad21, Smc1, and Smc3 molecules. The handcuff is established when two Rad21 molecules move into antiparallel orientation that is enforced by either SA1 or SA2. Sister chromatids are held together by one of the two rings. Inhibition of SA1/SA2 leads to dissociation and opening of the rings.

Results

To determine whether more than one set of cohesin subunits are in the cohesin holocomplex, we cloned the cDNA of cohesin subunits in frame into plasmids containing Flag, HA, or Myc epitope (Table S1, available at http://www.jcb.org/cgi/content/full/jcb.200801157/DC1) either at the NT or CT of the protein, coexpressed each cohesin subunit with two different epitopes, and used coimmunoprecipitation (IP) and Western blot (WB) analysis to delineate the inter- and intramolecular associations. The rationale was that the same cohesin subunit with different tagged epitopes should be able to immunoprecipitate each other if two copies of each cohesin subunit are in the cohesin holocomplex. Before performing the co-IP experiments, we extensively tested the transiently expressed cohesin proteins for their cellular localization (Fig. S1 A) and incorporation into the cohesin complex (Fig. S1 B) and validated the specificity of the IP studies (Fig. S1, C–D).

Each cohesin complex contains two Rad21 molecules

To investigate whether more than one Rad21 protein is in the cohesin complex, we coexpressed two Rad21 constructs with different epitopes in 293T cells, coimmunoprecipitated the protein, and analyzed the results using WB. The results indicate that Flag-Rad21 coimmunoprecipitates Myc-Rad21 and vice versa (Fig. 1 A). Moreover, WB with Rad21 pAb indicates that equal amounts of Myc-Rad21 and Flag-Rad21/endogenous Rad21 is coimmunoprecipitated (Fig. 1 A, right). It is possible that Myc-Rad21 forms a dimer with Flag-Rad21/endogenous Rad21 when Myc-Rad21 is underexpressed compared with Flag-Rad21/endogenous Rad21 (see next paragraph).

In addition to the co-IP of differentially tagged Rad21, we investigated whether ectopically expressed Rad21 could coimmunoprecipitate equal amounts of endogenous Rad21. We transfected HeLa cells with a 6×Myc-tagged Rad21 (Myc-Rad21) construct. In the Myc-Rad21 input control, the level of exogenous Myc-Rad21 was only 1/40 of the endogenous Rad21 (Fig. 1 B, left), but the same amount of endogenous Rad21 was coimmunoprecipitated by Myc-Rad21 (Fig. 1 B, right). This result suggests that approximately every molecule of Myc-Rad21 is incorporated into a protein complex with an endogenous Rad21 molecule and that each Myc-Rad21 coimmunoprecipitates one additional Rad21 molecule.

To determine whether Rad21–Rad21 interaction observed in the cohesin complexes also happens on the chromosome, we isolated chromatin and digested the DNA with micrococcal nuclease before co-IP experiments were performed. Similar to the previous experiments with whole cell lysates, co-IP experiments using either anti-Flag or Myc antibody agarose conjugates indicated that Myc-Rad21 can coimmunoprecipitate Flag-Rad21 and vice versa (Fig. S2 A, available at http://www.jcb.org/cgi/content/full/jcb.200801157/DC1), a finding that is consistent with the intermolecular association of Rad21 in whole cell lysate. Myc-Rad21 was also able to precipitate SA2 (Fig. S2 A), confirming that the ectopically expressed Rad21 protein is also associated with endogenous cohesin components.

To rule out any genomic DNA contamination in the cell lysates used in the IP experiments, cell lysates were prepared with and without nuclease (DNase I and/or RNase) treatment. The nucleic acid in the samples was isolated using phenol/chloroform extraction and amplified using random primer PCR. The results indicated that nucleic acid (DNA and RNA) could be amplified from the cell lysates in the absence of DNase I/RNase A (Fig. 1 C, lane 1). However, the amplified signal was reduced significantly when the lysates were treated with DNase I (Fig. 1 C, lane 2) or RNase A (Fig. 1 C, lane 3) and was completely eliminated by the treatment of both DNase I and RNase A (Fig. 1 C, lane 4). Compared with the signal from the positive control, which had 0.25 ng DNA as a template (Fig. 1 C, lane 10), the amount of DNA in the nuclease untreated cell lysate (125 µg of protein) was about the same (Fig. 1 C, lane 3), i.e., 1 ng DNA in 500 µg of protein. If the Rad21–Rad21 interaction shown in the co-IP experiments occurred via genomic DNA, we should have seen PCR-amplified DNA from the immunoprecipitated samples in the absence of nuclease treatment. However, random primer PCR results indicated that there was no DNA in the IP elutes, regardless of whether the cell lysates were treated with nuclease (Fig. 1 C, lanes 5 and 7) or not treated (Fig. 1 C, lanes 6 and 8). The co-IP results also showed that Flag-Rad21 and Myc-Rad21 can immunoprecipitate each other from either nuclease-treated or untreated samples (Fig. 1 D).

To further exclude the potential self-aggregation of Rad21 proteins, if any, Flag-Rad21 and Myc-Rad21 were expressed

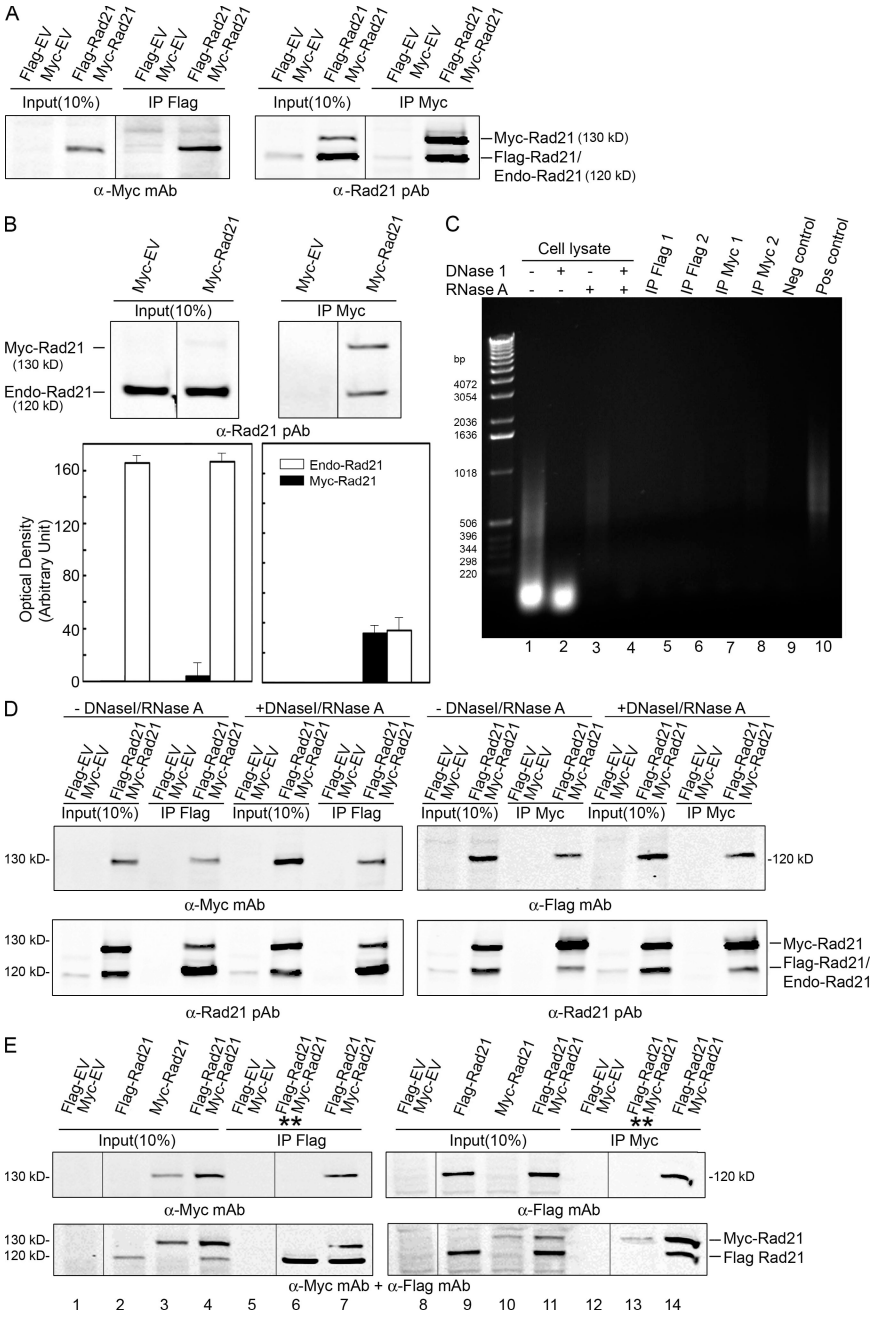

Figure 1. **Co-IP and WB analysis of cohesin Rad21–Rad21 interaction.** Logarithmically growing 293T or HeLa cells were transfected with appropriate Rad21 plasmids or empty vector (EV). Input (10% of IP) and IP samples were resolved by 7% SDS-PAGE and blotted with the indicated antibodies. (A) Flag-Rad21 and Myc-Rad21 coimmunoprecipitated. (B) Myc-Rad21 coimmunoprecipitated endogenous Rad21. Bar graphs show the relative level of Myc-Rad21 and endogenous Rad21 in input (left) and co-IP samples (right). Error bars indicate SEM from three observations. (C) Radom primer PCR amplification of DNA from 293T cell lysates and the elutes of immunoprecipitated samples. The template DNA used for PCR was purified from cell lysates after nuclease treatment as shown in lanes 1–4. The cell lysates for IP with Flag mAb (lanes 5 and 6) or Myc pAb (lanes 7 and 8) agarose-conjugated beads were digested with DNase I and RNase A in lanes 5 and 7 but were not digested in lanes 6 and 8. The amounts of DNA template used for PCR were from 125 μg of protein of cell lysates (lanes 1–4) or 1 mg of protein of cell lysates in IP samples (lanes 5–8). There is no DNA in the negative control (lane 9) and 0.25 ng DNA in the positive control (lane 10). (D) Cell lysates were treated with or without DNase I and RNase A before co-IP. (E) Co-IP of Flag-Rad21 and Myc-Rad21 from cells in which Flag-Rad21 and Myc-Rad21 were expressed separately, and lysates were mixed together before IP was performed (**, lanes 6 and 13) or from cells cotransfected with Flag-Rad21 and Myc-Rad21 (lanes 7 and 14). Black lines indicate that intervening lanes have been spliced out.

separately, and the cell lysates were mixed together before co-IP. The Flag-Rad21 and Myc-Rad21 mixture cannot be coimmunoprecipitated (Fig. 1 E, lanes 6 and 13), but coexpressed Flag- and Myc-Rad21 can be (Fig. 1 E, lanes 7 and 14). This result implies that co-IP of Flag-Rad21 and Myc-Rad21 is not caused by a simple aggregation, and, in intact cells, additional components may be required to form an intermolecular association of two Rad21 molecules.

Another approach to distinguishing specific association from nonspecific aggregation of ectopic Rad21 is to determine whether ectopic Rad21 can be efficiently incorporated into the cohesin holocomplex. SDS-PAGE with silver staining (Fig. S2 B, left) and WB (Fig. S2 B, right) indicate that Flag-Rad21 not only coimmunoprecipitates Myc-Rad21, which is shown as a distinct higher molecular weight band caused by 6×Myc epitope distinct from that of Flag-Rad21, but also coimmunoprecipitates other cohesin subunits, Smc1, Smc3, SA1, and SA2 (Fig. S2 B). Our mass spectrometry analysis of the immunoprecipitate from the DNase- and RNase-treated cell lysates verified that Flag-Rad21 indeed copurified Myc-Rad21 and the other core cohesin subunits (Fig. S2 C). Based on the aforementioned data (Fig. S2 and see preceding paragraph), we conclude that co-IP of Rad21 protein–protein interaction is specific and not caused by indirect association with genomic DNA or simple self-aggregation and multimerization, and there are two Rad21 molecules in each cohesin complex. These results provide the first indication that the cohesin complex in humans may not be a single ring but instead may be a dimeric or two-ring structure.

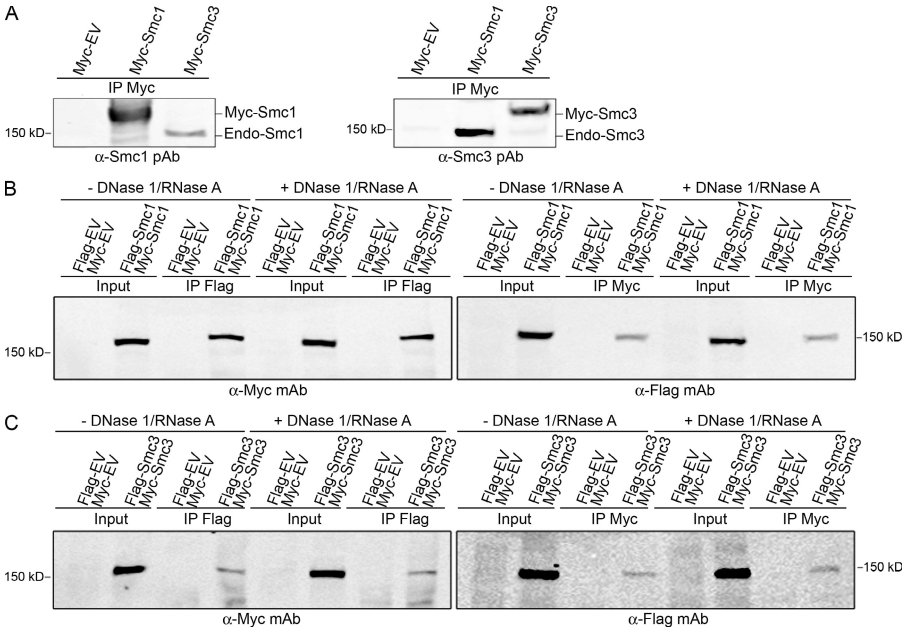

Figure 2. **Smc1 and Smc3 coimmunoprecipitate each other as well as themselves.** 293T cells were transfected with the appropriate plasmids. After 48 h, cell lysates were prepared and used for IP. The loaded input samples were equivalent to 10% of IP samples. (A) Myc-Smc1 and Myc-Smc3 coimmunoprecipitated endogenous Smc3 and Smc1 as well as endogenous Smc1 and Smc3, respectively. (B and C) Cell lysates were treated with or without DNase I and RNase A before co-IP of Smc1–Smc1 (B) and Smc3–Smc3 (C) was performed. EV, empty vector.

It has been reported that CT-tagged Scc1 with 18×Myc or 6×HA could not coimmunoprecipitate in yeast (Haering et al., 2002; Ivanov and Nasmyth, 2005), and Rad21-9×Myc could not coimmunoprecipitate endogenous Rad21 in stably transfected HeLa cells (Hauf et al., 2005). This finding is inconsistent with the results otained in this study using NT-tagged Rad21. Because an antibody against the last 14 aa residues of Rad21 only immunoprecipitates the free form of Rad21 and fails to immunoprecipitate Rad21 that has associated with Smc1–Smc3 (Fig. S3 A, available at http://www.jcb.org/cgi/content/full/jcb.200801157/DC1), the CT of Rad21 may be masked when Rad21 is incorporated into the cohesin complex. We hypothesize that tagging the Myc epitope to the CT of the Rad21 molecule might hinder the Rad21–Rad21 interaction. Using a bacterial artificial chromosome engineering system to tag 6×Myc epitopes at the NT of Rad21 (6×Myc-Rad21) or at the CT of Rad21 (Rad21-6×Myc), we made stable transfect 293 cell lines. We used Myc pAb–conjugated agarose beads to immunoprecipitate Myc-tagged Rad21. The result showed that only the NT Myc–tagged Rad21 can coimmunoprecipitate endogenous Rad21 (Fig. S3 B, lanes 7 and 8) but not the CT Myc–tagged Rad21 (Fig. S3 B, lanes 9 and 10). However, it is interesting to note that either NT- or CT-tagged Rad21 can coimmunoprecipitate the other cohesin components, such as Smc3 and SA2, indicating the presence of a different population and intermediates of the cohesin rings. This finding suggests that tagging epitopes to the CT of Rad21 molecules does not prevent single cohesin ring formation. These studies confirm that tagging the CT but not the NT of Rad21 with Myc epitopes affects the Rad21–Rad21 interaction.

Smc1 and Smc3 coimmunoprecipitate themselves

Next, we tested whether more than one copy of Smc1 and Smc3 proteins is in the cohesin complex by using a strategy similar to the one used in studying Rad21–Rad21 interaction. It has been previously shown that the cohesin complex contains Smc1 and Smc3 and that they form a heterodimer via their hinge domain (Haering et al., 2002). In the cohesin complex, Smc1 and Smc3 heads are also tethered by Rad21 CT and NT, respectively (Gruber et al., 2003, 2006). In either case, Smc1 and Smc3 proteins should coimmunoprecipitate, and this is confirmed by our data (Fig. 2 A). Our co-IP studies indicated that Myc-Smc1 and Myc-Smc3 also coimmunoprecipitate endogenous Smc1 and Smc3, respectively, which are shown as faint bands under Myc-Smc1 and Myc-Smc3 bands (Fig. 2 A).

To further verify whether Smc1 and Smc3 can coimmunoprecipitate themselves, Smc1 and Smc3 were tagged with Flag and Myc epitopes. After cotransfection of cells with Flag-Smc1 and Myc-Smc1 plasmids, reciprocal co-IP was performed. WB results showed that Flag-Smc1 reciprocally coimmunoprecipitated Myc-Smc1. Similar results were obtained for Flag-Smc3 and Myc-Smc3 (unpublished data). As previously shown for Rad21, to exclude the possibility that Myc- and Flag-tagged Smc1 and Smc3 coimmunoprecipitate themselves via genomic DNA that might present as contaminants in protein lysates, we treated cell lysates with DNase I and RNase A before co-IP. The results from DNase I– and RNase A–treated samples were very similar to those from samples without DNase I and RNase A treatment (unpublished data); i.e., Flag-Smc1 and Myc-Smc1 reciprocally coimmunoprecipitate (Fig. 2 B), as do Flag-Smc3 and Myc-Smc3 (Fig. 2 C). Co-IP of Myc- and Flag-Smc1 as well as Myc- and Flag-Smc3 is therefore not caused by nonspecific association with the genomic DNA. These findings suggest that there is more than one copy of Smc1 and Smc3 molecules in the cohesin complex.

Each cohesin complex contains one molecule of SA1 or SA2

In budding yeast, Scc3 is a core subunit of the cohesin complex. In humans, there are two orthologues of Scc3, SA1 and SA2, and SA2 is more abundant than SA1 (Losada et al., 2000). Because three of the four cohesin core subunits, Rad21, Smc1,

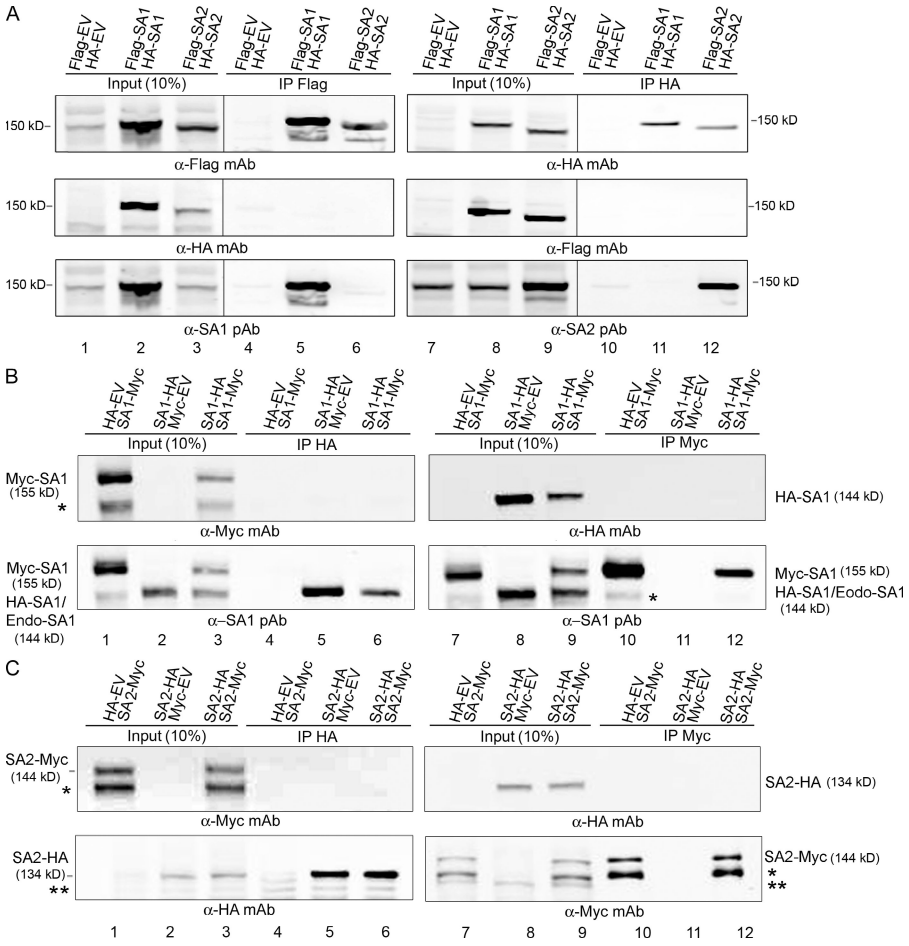

Figure 3. **Each cohesin complex contains only one copy of SA1 or SA2.** 293T cells were cotransfected with the respective constructs. 48 h after transfection, IP was performed. SA1 and SA2 were detected using the corresponding antibodies shown on the blots. (A) HA and Flag epitopes were tagged to the NT of SA1 and SA2. (B and C) HA and Myc epitopes were tagged to the CT of SA1 and SA2. EV, empty vector; *, splicing SA1-Myc or SA2-Myc; **, nonspecific band. Black lines indicate that intervening lanes have been spliced out.

and Smc3, can immunoprecipitate themselves, the cohesin complex might contain more than one copy of the fourth core subunit, SA1/SA2. To investigate whether SA1 can immunoprecipitate itself, we cotransfected 293T cells with Flag-SA1 and HA-SA1 constructs. An IP experiment using asynchronous 293T cells demonstrates that Flag-SA1 and HA-SA1 cannot coimmunoprecipitate (Fig. 3 A, lanes 5 and 11). The inability to detect an interaction between Flag-SA1 and HA-SA1 was not caused by failure of the IP, as Flag and HA antisera efficiently detected the bands of Flag-SA1 and HA-SA1, respectively (Fig. 3 A). We also obtained similar results when Flag-SA1 and Myc-SA1 were used in co-IP experiments (unpublished data). Similar to SA1, neither Flag-SA2 or HA-SA2 (Fig. 3 A, lanes 6 and 12) nor Myc-SA2 or Flag-SA2 (not depicted) can immunoprecipitate each other.

As shown above (see preceding paragraphs), in the case of Rad21, tagging an epitope to the different ends of a protein may affect the protein–protein interaction. To rule out the lack of a self-interaction in SA proteins caused by the NT tagging, we generated a set of SA constructs with HA and Flag tagged to the CT of the molecule and used co-IP to investigate the interaction of SA1–SA1 as well as SA2–SA2. Similar to the NT-tagged SA proteins, both CT-tagged SA1-HA and SA1-Myc (Fig. 3 B, lanes 6 and 12) and SA2-HA and SA2-Myc failed to coimmunoprecipitate (Fig. 3 C, lanes 6 and 12), suggesting a lack of a detectable SA–SA self-interaction. However, we cannot rule out the possibility that either NT- or CT-tagged SA could hinder SA–SA self-interaction. Alternatively, the SA–SA interaction does exist in vivo, but it is so weak that we fail to detect the interaction using co-IP.

We further investigated the possible interactions between SA1 and SA2 (Fig. 3 A, lanes 6 and 11), and our data are consistent with the results that SA1 and SA2 do not coexist in the same cohesin complex as reported previously (Losada et al., 2000; Sumara et al., 2000). In co-IP experiments using synchronized HeLa cells, we confirmed that association of one molecule of SA1 or SA2 to the cohesin complex is not affected by the stages of the cell cycle (unpublished data). This set of experiments suggests that, unlike other cohesin units (Rad21, Smc1, and Smc3), there is only one molecule of SA1 or SA2 in each cohesin complex.

Rad21–Rad21 oriented in an antiparallel manner in cohesin holocomplex

To investigate how Rad21 proteins interact with each other, we used a fluorescence PCA, a technique that has been widely used to study the dynamics of protein–protein interactions (Michnick, 2003; Remy and Michnick, 2003). Enhanced YFP was used in this study. YFP is split into two pieces, YFP(NT) (157 aa) and YFP(CT) (81 aa). Wild-type Rad21 was cloned into the PCA vectors, resulting in four different fusion proteins, i.e., YFP(NT)-Rad21, YFP(CT)-Rad21, Rad21-YFP(NT), and Rad21-YFP(CT).

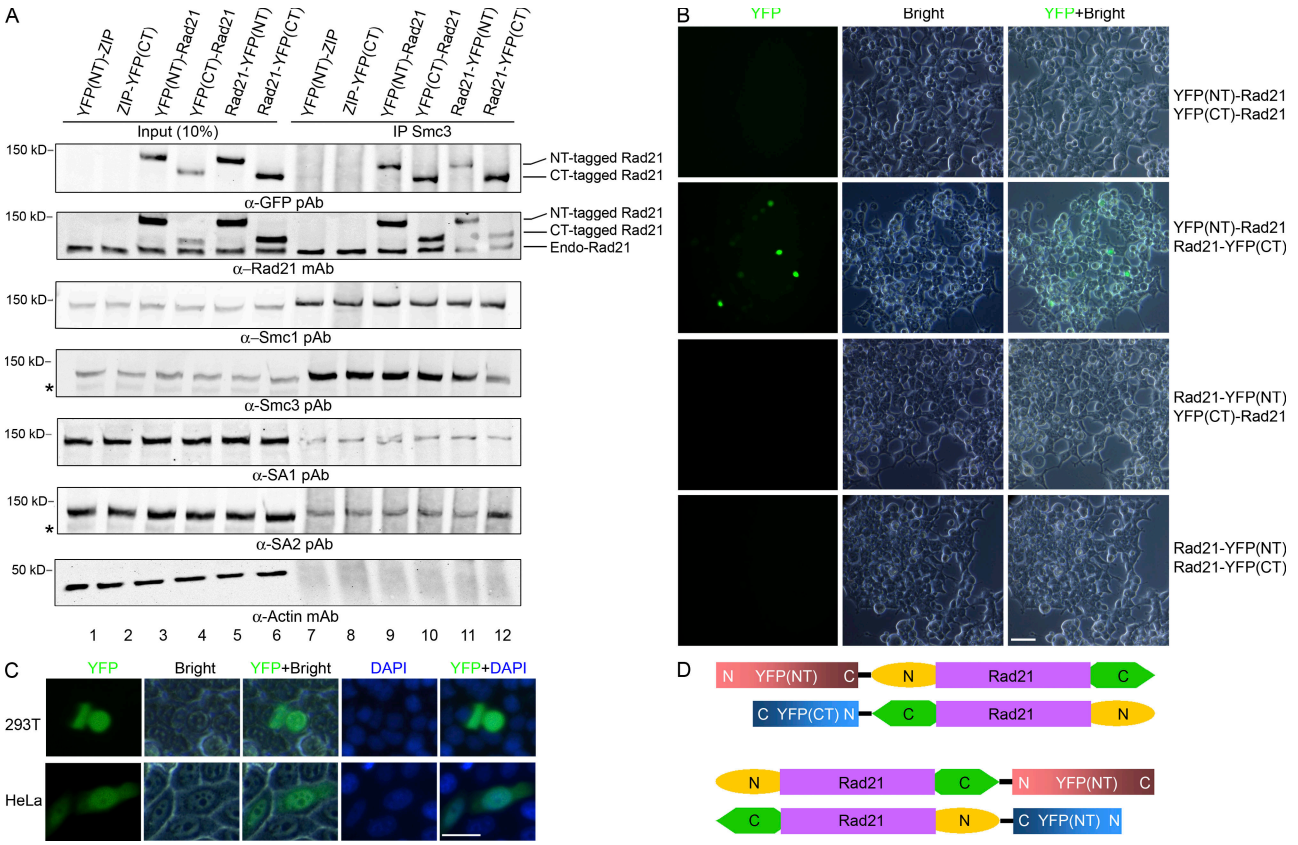

Figure 4. **Fluorescent protein fragment complementation assay showing the Rad21–Rad21 interaction and the antiparallel orientation.** (A) YFP(NT) or YFP(CT) were fused to either the NT or CT end of Rad21. YFP-fused Rad21 constructs were expressed in 293T cells (lanes 3–6), and their interaction with the cohesin complex was examined by IP of the endogenous Smc3 using rabbit anti-Smc3 antisera (lanes 9–12). *, nonspecific band. (B) 293T cells were cotransfected with YFP(NT)- and YFP(CT)-fused Rad21 plasmids (a total of four combinations). YFP fluorescence was examined under a fluorescent microscope 40 h after transfection. (C) YFP fluorescence–positive 293T and HeLa cells transfected with the combination of YFP(NT)-Rad21 and Rad21-YFP(CT) at 400× magnification. (D) Possible antiparallel orientation of Rad21–Rad21 interactions. Only the combination of plasmids in the top panel results in the fluorescence. Bars, 25 μm.

Using Smc3 pAb, we tested the expression of the YFP fragment–fused Rad21 molecules in 293T cells and their incorporation into the cohesin complex by immunoprecipitating endogenous Smc3 (Fig. 4 A). All YFP-fused Rad21 are expressed (Fig. 4 A). YFP(CT)-Rad21 could not be detected as efficiently by the GFP pAb as the other three YFP-fused Rad21. However, the level of YFP(CT)-Rad21 is found to be equivalent to endogenous Rad21 when the blot was probed with Rad21 mAb (Fig. 4 A, lane 4). IP of endogenous Smc3 using Smc3 pAb not only efficiently coimmunoprecipitated all four YFP-fused Rad21 proteins but also coimmunoprecipitated endogenous Rad21 (Fig. 4 A, lanes 9–12) along with the other cohesin subunits Smc1, SA1, and SA2 (Fig. 4 A). The four YFP-tagged Rad21 and the other three cohesin core subunits, Smc1, Smc3, and SA1/2, can also be immunoprecipitated by GFP pAb (Fig. S4, available at http://www.jcb.org/cgi/content/full/jcb.200801157/DC1). These data suggest that exogenously YFP-fused Rad21 can be incorporated into the cohesin complex as endogenous Rad21.

To investigate whether Rad21-fused YFP(NT) and YFP(CT) can fold into a state that emits yellow fluorescence as full-length YFP, we cotransfected 293T and HeLa cells with one of the two YFP(NT)-fused Rad21 constructs and one of the two YFP(CT)-fused Rad21 constructs, which yielded four combinations (Fig. 4 B). Out of the four combinations, we observed only YFP fluorescence in the cells transfected with plasmids containing YFP(NT)-Rad21 and Rad21-YFP(CT) cDNAs (Fig. 4, B and C). The YFP fluorescence is not likely to be caused by nonspecific aggregation of YFP(NT)-Rad21 and Rad21-YFP(CT) because the other three cotransfection combinations also have both YFP(NT) and YFP(CT) fragments, but no YFP fluorescent signal was observed in any of these (Fig. 4 B). The absence of YFP fluorescence in the combination of YFP(NT)-Rad21 and YFP(CT)-Rad21 as well as Rad21-YFP(NT) and YFP(CT)-Rad21 should not be caused by relatively low expression of YFP(CT)-Rad21 (Fig. 4 A, lane 4) because the amount of YFP(CT)-Rad21 incorporated into the cohesin complex (Fig. 4 A, lane 10) is similar to that of the other three YFP-fused Rad21 (Fig. 4 A, lanes 9, 11, and 12) when they were coimmunoprecipitated by Smc3 pAb. Moreover, we did not observe a YFP signal in the combination of Rad21-YFP(NT) and Rad21-YFP(CT) despite the good expression of Rad21-YFP(CT) (Fig. 4 A, lane 6). These results provide two important clues that indicate how Rad21 proteins orient in the cohesin complex (Fig. 4 D). First, the two Rad21 molecules are next to each other because the YFP(NT) and YFP(CT) fused to Rad21 proteins have to be brought close enough to fold into a functional

fluorescence-emitting configuration (Fig. 4 D, top). Second, the two Rad21 proteins align in an antiparallel manner because, to assemble a functional YFP molecule, YFP(NT)-Rad21 and Rad21-YFP(CT) have to be brought together; i.e., the CT of one Rad21 protein is close to the NT of another Rad21 protein (Fig. 4 D, top). The fragments of YFP in Rad21-YFP(NT) and YFP(CT)-Rad21 can also be brought together (Fig. 4 D, bottom), but fluorescence was not observed (Fig. 4 B). It is possible that the reverse polarity of YFP(NT) and YFP(CT) fused to Rad21 may hinder the appropriate folding of YFP and Rad21–Rad21 interaction (Fig. 4 D, bottom). These findings suggest that two cohesin rings are dimerized via the two Rad21 subunits that exist in an antiparallel orientation in the cohesin holocomplex.

The percentage of cells with YFP fluorescence was low, only ~3–5% (Fig. 4 B), whereas the transfection efficiency was ~80% when the cells were cotransfected with pDsRed2-C1 plasmid, which expresses RFP. The discrepancy between the high transfection rate in cells transfected with control plasmid and the observed YFP-positive cells transfected with YFP(NT)-Rad21 and Rad21-YFP(CT) is possibly a result of the structural hindrance caused by the CT tag of Rad21-YFP(CT) that fails to dimerize with YFP(NT)-Rad21, which is similar to that seen in the earlier IP experiments (Fig. S3 B). Another possibility is that endogenous Rad21 competes with the YFP(NT)- or YPF(CT)-tagged Rad21 to form Rad21–Rad21 dimers. It is less likely that the YFP fluorescence resulted from two proximate cohesin complexes with YFP(NT)-Rad21 and Rad21-YFP(CT) because the two adjacent YFP(NT)-Rad21 and Rad21-YFP(CT) have the same reverse polarity dilemma as discussed in the preceding paragraphs.

In our previous yeast two-hybrid assay using Rad21 NT long (NT-L; 1–283 aa) and CT long (CT-L; 254–631 aa) as bait, we isolated full-length Rad21 as an interactor (unpublished data). To further verify the interaction of Rad21–Rad21 shown in the aforementioned co-IP and PCA studies, we extended our yeast two-hybrid assay as additional evidence. The cDNAs of full-length Rad21, Rad21 NT-L, Rad21 CT-L, and Rad21 CT (450–631 aa) were cloned into *GAL4* DNA–binding (pC97) and *GAL4* DNA activation (pC86) domain plasmids. WB results show that the constructs are well expressed in the two-hybrid yeast stain MV103 (Fig. 5 A). A yeast two-hybrid assay demonstrates that full-length Rad21, Rad21 NT-L, and Rad21 CT-L interact with themselves and with each other (Fig. 5 B). However, NT-truncated Rad21 (Rad21 CT) failed to interact with itself or with other Rad21 constructs (Fig. 5 B), which is consistent with the IP results (not depicted). Based on the findings in PCA and yeast two-hybrid assay, we conclude that Rad21 interacts with Rad21 and aligns in an antiparallel manner in the cohesin complex.

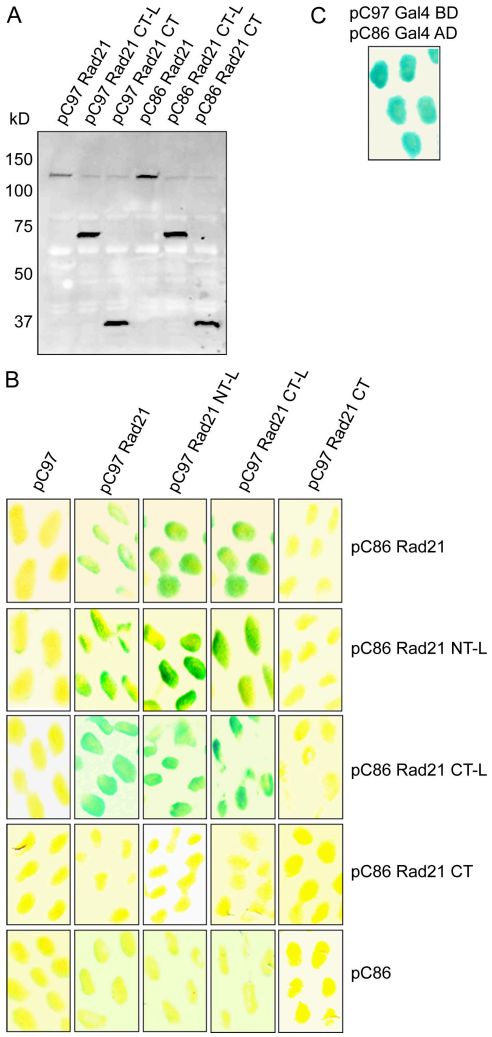

Figure 5. **Rad21–Rad21 interaction determined by yeast two-hybrid assay.** (A) Expression of Rad21 wild type (1–631 aa), CT-L (254–631 aa), and CT (451–631 aa) in yeast was analyzed with WBs using Rad21 CT–specific pAb. (B) A *LacZ* reporter assay was used to probe the Rad21–Rad21 interaction. Yeast cells cotransfected with pC97 and pC86 empty vector is shown as the negative control. (C) pC97 *GAL4*BD and pC86 *GAL4*AD were used as the positive control. Positive protein–protein interaction is shown in blue in th *LacZ* reporter assay.

Inhibition of SA1 and SA2 prevents Rad21-Rad21 interaction and causes loss of sister chromatid cohesion

Our IP data indicate that the interaction of Rad21 with Rad21 (Figs. S2 and S3) or full-length Rad21 with some truncated Rad21 products (not depicted) is always associated with SA1/SA2. We hypothesized that SA1 or SA2 is one of the linkers of the two Rad21 molecules of the cohesin rings and tested this hypothesis using SA1 and SA2 siRNA. SA1 and SA2 proteins are reduced by 65% and 75%, respectively, with siRNA treatment (Fig. 6, A [lanes 3 and 4] and B [lanes 2 and 3]). In multiple experiments, co-IP of endogenous Rad21 by Myc-Rad21 was significantly reduced by SA2 inhibition, whereas SA1 siRNA treatment had a lesser effect (Fig. 6 A). We performed an additional experiment by cotransfecting Flag-Rad21 and Myc-Rad21 and coimmunoprecipitating the epitope-tagged Rad21 (Fig. 6 B). Similar to the results shown in Fig. 6 A, in this cotransfection experiment, the knockdown of SA2 by siRNA blocked the co-IP of Flag-Rad21 and Myc-Rad21 (Fig. 6 B, lanes 7, 8, 11, and 12). These results suggest that SA2 may play a role in locking the two associated Rad21 molecules, and they are also consistent with the data that SA2 is the dominant form of Scc3 in human somatic cells (Losada et al., 2000). It is interesting to note that although the interaction between the two rings is lost, the

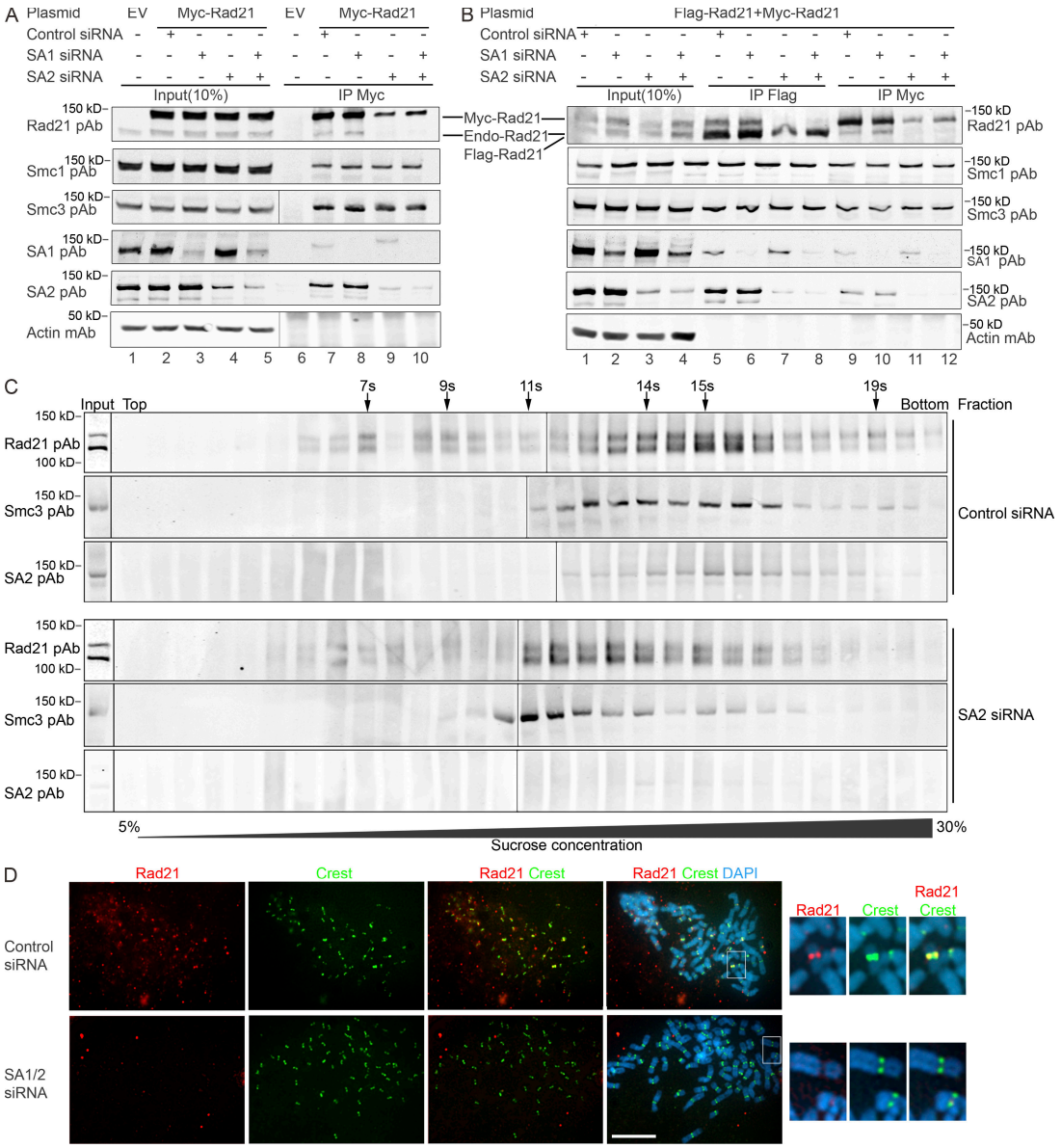

Figure 6. **Knockdown of SA1/SA2 disrupts the Rad21–Rad21 interaction and the formation of the two-ring cohesins.** (A and B) SA1 and SA2 are knocked down by respective siRNA 24 h after transfection with tagged Rad21 into 293T cells. (A) Myc-Rad21 cannot coimmunoprecipitate endogenous Rad21 when SA2 is knocked down. (B) Myc-Rad21 and Flag-Rad21 cannot reciprocally coimmunoprecipitate each other when SA2 is down-regulated. (C) Sucrose gradient centrifugation to study cohesin–cohesin interaction after SA2 knockdown. 293T cells were transfected with SA2 siRNA or control siRNA, and, 24 h later, the cells were cotransfected with Myc-Rad21 and Flag-Rad21 for 40 h. Cell lysates were prepared and used in sucrose gradient centrifugation. Rad21, Smc3, and SA2 were analyzed using WB. Sedimentation coefficient is shown on the top of the blot. Input, sample before sucrose gradient centrifugation. (D) Dissociation of cohesin from sister chromatids in SA2 knockdown cells. HeLa cells in the mitosis phase were cytospun onto slides, and immunofluorescent microscopy was performed. Rad21 mAb and human CREST antibodies were used to probe Rad21 (red) and centromere (green), respectively. The nuclear material is visualized by DAPI staining (blue). The centromeres of one chromosome shown in the boxes of merge panels are enlarged on the right. (A and C) Black lines indicate that intervening lanes have been spliced out. Bar, 10 μm.

three core subunits, Rad21, Smc1, and Smc3, remained associated, as Myc-Rad21 could still coimmunoprecipitate Smc1 and Smc3 (Fig. 6, A [lanes 9 and 10] and B [lanes 7, 8, 11, and 12]), suggesting an intact one-ring cohesin complex. The immunofluorescence microscopy also demonstrates that Rad21 and Smc3 colocalize in SA1 and SA2 knockdown cells (Fig. S5, available at http://www.jcb.org/cgi/content/full/jcb.200801157/DC1), further supporting the association of Rad21, Smc1, and Smc3 and suggesting that both one-ring and two-ring cohesin complexes can exist in the same cells.

To further characterize the role of SA2 in the cohesin complex, we used sucrose gradient centrifugation to investigate the different forms of cohesin. The rationale was that a cohesin complex with fewer subunits (e.g., single ring) will sediment more slowly than one with more subunits (e.g., double ring). Therefore, different populations of cohesins can be separated with sucrose gradient centrifugation. We knocked down SA2 before the cells were transfected with Myc-Rad21 and Flag-Rad21. After the cell lysate was ultracentrifuged, the sample was fractionated, and cohesin subunits in each fraction were analyzed using WBs.

As shown in Fig. 6 C (input lane), SA2 in SA2 siRNA–treated cells is reduced by ∼90% compared with the control. Both control and SA2 knockdown samples have fractions containing only Rad21, Rad21–Smc3, and Rad21–Smc3–SA2, suggesting mixed populations of cohesin complexes/subunits. In both the control and SA2 knockdown samples, most Rad21 molecules were detected in the same fraction as Smc3. However, the migration of Rad21–Smc3 in the SA2 siRNA–treated sample (11–12 s) was slower than that of the control (14–15 s; Fig. 6 C), which is likely caused by the absence of the SA2 protein in the SA2 siRNA–treated sample. We also found a minor cohesin population around 19 s in the control sample, which does not exist in the SA2 knockdown sample (Fig. 6 C, bottom). Because SA2 knockdown leads to the failure of Rad21–Rad21 interaction (Fig. 6, A and B), the cohesin population in the fractions around 19 s in the control sample may represent the dimeric cohesin complex, whereas the cohesin population in the fractions around 14 s represents the single-ring cohesin (Fig. 6 C, top), and the cohesin population in the fractions around 11 s in the SA2 knockdown sample represents the single-ring cohesin without SA2 (Fig. 6 C, bottom). Because sucrose gradient centrifugation alone cannot determine the molecular weight of an asymmetrical protein like cohesin, the fraction that contains the dimeric cohesin complex remains to be determined.

To determine whether the rings consisting of Rad21, Smc1, and Smc3 are on the sister chromatids after SA2 knockdown, we performed immunostaining to visualize any cohesin signals on chromosomes by using Rad21 and SA2 antisera. In prometaphase and metaphase cells treated with control siRNA, Rad21 signals (Fig. 6 D, red) were found on the centromeres, which were colocalized with CREST centromere antigen (Fig. 6 D, green). However, the Rad21 signal on the centromere was significantly reduced or completely absent in SA2 siRNA–treated cells (Fig. 6 D). Similar to Rad21, SA2 signals were found on centromeres in the control but were completely absent in SA2 siRNA–treated cells (unpublished data). These results suggest that cohesin rings are opened and disassociated from sister chromatids once SA2 is knocked down. In summary, based on our biochemical and cytogenetic analyses, we conclude that SA1 and SA2 may serve as the locking device that holds the two cohesin rings together. Inhibition of these locking molecules not only dissociates the two rings but also opens them up.

Discussion

The Rad21–Rad21 interaction is the cornerstone of our handcuff model. Our analysis of the cohesin ring arose from two unexpected observations: (1) the isolation of Rad21 as an interactor in a two-hybrid assay using several different Rad21 baits (NT-L, CT-L, and full length) and (2) co-IP of endogenous or differentially tagged Rad21. These results lead us to hypothesize that Rad21 interacts with itself, and this interaction forms a basis for a higher order cohesin complex.

The one-ring embrace model proposes that cohesin complexes are loaded to the chromosome before the S phase, sister chromatid cohesion is established after the replication fork passes through the cohesin ring during DNA replication, and cohesion is dissolved when cohesin subunit Scc1/Mcd1/Rad21 is cleaved by separase at the onset of the metaphase to anaphase transition (Gruber et al., 2003; Haering and Nasmyth, 2003; Uhlmann, 2004). With the accumulation of data from recent studies using budding yeast and other organisms (Stead et al., 2003; Chang et al., 2005; Guacci, 2007; Surcel et al., 2008; Yeh et al., 2008), the one-ring model faces increasing challenges from alternative models. The one-ring model has several caveats, including the static configuration of the cohesin ring, which cannot properly explain how sister chromatid cohesion is established during DNA replication in the S phase, how genome-wide cohesion is generated once a double-strand DNA break happens in the G2/M phase, and how transcription is regulated. On the contrary, a two-ring model in which cohesin complexes associate with each sister chromatid that becomes paired during DNA replication is a valid alternative because it can accommodate the drawbacks of the one-ring embrace model.

Handcuff model for cohesin

Our data show that there is a population of cohesin subunits that immunoprecipitate themselves in an Scc3 (SA1/SA2)-dependent manner. Three of the four core subunits, Rad21, Smc1, and Smc3, not only immunoprecipitate each other but also immunoprecipitate themselves. The ratio of Myc-Rad21 pulling down Flag-Rad21 and/or endogenous Rad21 is 1:1. Furthermore, Rad21–Rad21 interaction is also observed in a yeast two-hybrid assay. These results provide the first indication that the cohesin complex in humans may exist as a dimeric or a two-ring structure.

Although several dimeric ring models (Fig. 7, A–C) have been proposed (Campbell and Cohen-Fix, 2002; Stead et al., 2003; Huang et al., 2005; Nasmyth, 2005; Skibbens, 2005; Guacci, 2007; Skibbens et al., 2007), until now there has been no direct experimental evidence supporting these models. PCA experiments have provided two valuable clues about how Rad21 proteins interact. First, the two Rad21 molecules must have close proximity to each other in the cohesin complex. Otherwise, the YFP(NT) and YFP(CT) fragments would be unable to fold into a configuration to emit fluorescence. This close proximity prompted us to challenge the two dimeric models in which two Smc1–Smc3 heterodimers are connected by two Rad21 molecules that are on opposite sides of the ring (Fig. 7 A), or Rad21 tethers the Smc1 and Smc3 heads that belong to two different Smc1–Smc3 heterodimers (Fig. 7 B). The second clue is that the two Rad21 proteins align in an antiparallel fashion such that the YFP(NT) in YFP(NT)-Rad21 and the YFP(CT) in Rad21-YFP(CT) can be close enough to form a fluorescence-emitting configuration. These findings collectively suggest that two cohesin rings are either directly or indirectly dimerized via Rad21 subunits (Fig. 7 C).

The possible dimerization of cohesin rings in yeast and humans has been studied in the past using co-IP approaches similar to ours and most recently using fluorescence resonance energy transfer (FRET; Mc Intyre et al., 2007). The earlier co-IP studies might have missed this important interaction because of their use of the C-terminally tagged Scc1/Mcd1/Rad21 constructs (Haering et al., 2002; Hauf et al., 2005). As we have shown, the CT

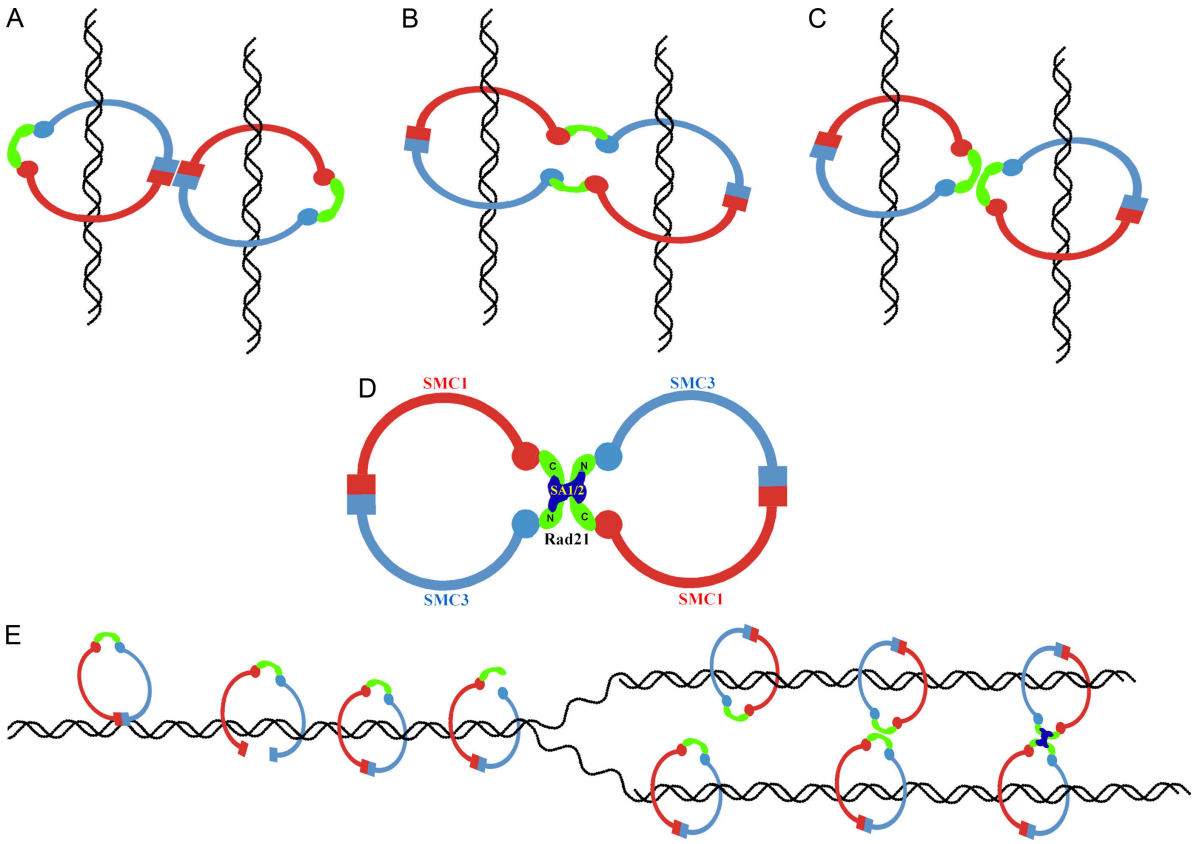

Figure 7. **Handcuff model of cohesin complex.** (A–C) Different configurations of two-ring models. (D) Handcuff model consists of two rings. (E) Establishment of sister chromatid cohesion. For simplicity, only cohesin complexes are shown on the model. Single-ring cohesin complexes are loaded onto the chromosomes at any stage of the cell cycle. During DNA replication at S phase, each of the rings entraps one chromatin. The handcuff is established when the two Rad21 molecules are paired and tethered either by SA1 or SA2 via interaction with the two Rad21 molecules.

domain is masked once Rad21 is incorporated into the cohesin complex. Including a tag in this domain can still form a single-ring cohesin complex but may significantly inhibit the formation of a two-ring cohesin complex or significantly weaken the association affinity of the two rings such that the components of the two cohesin rings cannot be coimmunoprecipitated. It may also account for the low positive rate in our PCA experiment. The possible weak association of two cohesin rings with a CT tag in vivo may also explain why earlier studies (Haering et al., 2002; Hauf et al., 2005) failed to see the interaction between Scc1/Mcd1/Rad21 and why in these experiments budding yeast cells were viable when they contained only CT-tagged Mcd1–Scc1–Rad21. In their FRET assay (Mc Intyre et al., 2007), CFP and YFP were conjugated to the two Smc1/Smc3 heads or hinge domains, respectively. The authors excluded the possibility of dimerization of two cohesins via the hinge domain (Mc Intyre et al., 2007), which is consistent with our data. Although the head-to-head interaction of two Smc1–Smc3 heterodimers has not been found via FRET, the result is not conclusive because the two heterodimers might be separated by other proteins, such as Rad21, Scc3, etc., and may be too far apart to produce FRET. Surprisingly, the possible Rad21–Rad21 dimerization was not tested with FRET in their study (Mc Intyre et al., 2007).

What leads to the dimerization of two cohesin rings? The Rad21–Rad21 interaction in yeast two-hybrid assay and co-IP of the full-length and truncated Rad21 proteins themselves (unpublished data) along with SA1 and SA2 indicate that the interaction between two Rad21 molecules is stabilized by SA1 or SA2. Inhibition of the Rad21–Rad21 co-IP and premature separation of sister chromatids caused by SA1 and SA2 knockdown (unpublished data) further strengthen the notion that SA1 and SA2 are indeed one of the molecules that link the two cohesin rings. Disruption of the linkers (SA1/SA2) between the two rings abolishes cohesion by disrupting the Rad21–Rad21 interaction, resulting in the dissociation of the two rings. However, we do not exclude the possibility that other cohesin-associating proteins along with SA1 and SA2 may play a role in the dimerization of the two cohesin rings. For instance, Pds5 is found to bind to both Scc1/Mcd1/Rad21 and the hinge of Smc1–Smc3 in budding yeast (Mc Intyre et al., 2007). It has been shown to maintain sister chromatid cohesion and is implicated in helping to form a dimeric cohesin ring (Stead et al., 2003; Guacci, 2007; Skibbens et al., 2007). We also found that Pds5 was coimmunoprecipitated when Rad21 copurified itself (unpublished data). Therefore, Pds5 might be one of the proteins that help SA1 and SA2 to maintain the dimeric rings.

Our results and data from other laboratories (Losada et al., 2000; Sumara et al., 2000) indicate that SA1 and SA2 do not exist in the same cohesin complex and that each cohesin complex contains only one molecule of SA1 or SA2. These data support

the model that cells have two types of cohesin complexes, cohesin$^{(SA1)}$ and cohesin$^{(SA2)}$, containing either SA1 or SA2, respectively. SA1 and SA2 are the possible locking/bridging molecules that bring the two rings together by tethering the two Rad21 molecules aligned in an antiparallel manner via interactions with Rad21 molecules.

Based on these analyses, we are outlining a handcuff model of cohesin complexes (Fig. 7 D). The handcuff model consists of two rings; each of the rings contains one set of Rad21, Smc1, and Smc3 molecules. Smc1 and Smc3 form a heterodimer, and Rad21 CT and NT bind to the heads of Smc1 and Smc3, respectively. SA1 or SA2 links the two rings via interaction with Rad21. In addition to the cohesin core subunits, other cohesin associate proteins, such as Pds5, may also help in the formation of the two-ring cohesin structure.

How is sister chromatid cohesion established?

The association of the cohesin complex with chromosome requires the cohesin-loading complex Scc2–Scc4 (Ciosk et al., 2000; Gillespie and Hirano, 2004; Strom et al., 2004; Takahashi et al., 2004; Watrin et al., 2006; Gause et al., 2008; Misulovin et al., 2008), and EcoI/Ctf7 is essential for the establishment of sister chromatid cohesion (Skibbens, 2005; Skibbens et al., 2007; Unal et al., 2007). The two-ring model proponents argue that cohesin rings are loaded to chromosome before DNA replication can be distributed to sister chromatids and paired by EcoI/Ctf7 to establish cohesion. It was believed that sister chromatid cohesion is established by entrapping the ring after DNA replication via the opening of the Smc3 head and the Rad21 NT (Uhlmann, 2004), but a recent study indicates that the DNA is loaded via the opening of Smc1 and Smc3 hinges (Gruber et al., 2006). We propose that cohesin rings are loaded onto the chromosomes by the Scc2–Scc4 loading complex via the opening of the Smc1–Smc3 hinge. Each ring passes through the replication fork by opening the Smc3 head and the NT of Rad21 and is located to one of the two sister chromatids. The cohesin rings can also be recruited to the newly replicated sisters from a cellular cohesin pool if the amount of preexisting cohesin on the chromosomes is not sufficient. When a double-strand DNA break occurs, cohesin rings are loaded onto the damaged chromosome as well as to the undamaged chromosome. The cohesion of sister chromatids is established with the help of EcoI/Ctf7 when the two rings are locked by pairing the two Rad21 molecules in an antiparallel manner, tethered by SA1 or SA2, and possibly assisted by other cohesion-maintaining proteins (Fig. 7 E).

How does cohesin dissociate from chromosomes?

In the normal cell cycle, the removal of cohesin from sister chromatids in budding yeast is different from that in metazoa. In *S. cerevisiae*, cohesin complexes embrace both sister chromatids together until metaphase to anaphase transition (Haering and Nasmyth, 2003). All cohesin complexes are removed from chromosomes simultaneously when separase cleaves the cohesin subunit Scc1/Mcd1 (Cohen-Fix et al., 1996; Ciosk et al., 1998). However, a recent study showed that the budding yeast pericentric chromatin is organized into a cruciform in mitosis; i.e., centromere-flanking DNA adopts an intramolecular loop, whereas sister chromatid arms are still paired intermolecularly (Yeh et al., 2008). Fluorescence microscopy data suggest that the cohesins on the intramolecular centromeric chromatin loop are from intermolecular sister chromatid arms. It is difficult to explain this finding if sister chromatid is circled by a one-ring cohesin complex. However, it can be explained through our handcuff cohesin model. If each of the sister chromatids are held by one cohesin ring and the two cohesins are dimerized by Scc3 during anaphase, the paired cohesin complexes on sister chromatids are dissociated from each other via postmodification of Scc3. The one-ring cohesin flanking the centromere becomes paired during the formation of the intramolecular loop.

Most other eukaryotes, including mammals, are different from budding yeast in cohesin removal during the mitosis (Waizenegger et al., 2000). The bulk of the cohesin complexes along the chromosome arms dissociates during prophase (Sumara et al., 2000; Gimenez-Abian et al., 2004). This step is dependent on the activity of PLK1 and aurora B and independent of separase activation (Sumara et al., 2002; Gimenez-Abian et al., 2004; Hauf et al., 2005). PLK1 and aurora B destabilize cohesin complexes via the phosphorylation of SA2. Cohesin with SA2 phosphorylation mutant subunit cannot be removed from the chromosome arm during prophase (Hauf et al., 2005). The removal of cohesin from the chromosomal arm during prophase via the phosphorylation of SA2 fits well in our handcuff model because this model predicts that SA1 and SA2 are the linking proteins that pair the two one-ring cohesins. However, it seems unnecessary for cohesin rings to dissociate from the chromosome arms during prophase if each of the sisters is held by one of the cohesin rings. It is possible that phosphorylation of SA2 not only unlocks the two cohesin rings but also destabilizes the entire ring, causing the cohesin components to be removed from the chromosome. The advantage of this mechanism is to prevent arm chromatid from becoming cohesed again before the onset of anaphase when separase cleaves the centromeric and any leftover cohesins along the chromosome arms (Hauf et al., 2001; Haering and Nasmyth, 2003; Nakajima et al., 2007).

In summary, a two-ring handcuff model for the cohesin complex is not only flexible enough to establish and maintain sister chromatid cohesion but can also ensure the fidelity of chromosome segregation in higher eukaryotes. How the cohesion of sister chromatids is established by the two-ring handcuff model during DNA replication and DNA double-strand break repair remains to be elucidated and will be the focus of a future investigation.

Materials and methods

Antibodies

The sources of pAbs used are as follows: Flag (Sigma-Aldrich), Rad21 (Pati et al., 2002), Smc3 (Bethyl Laboratories, Inc.), Smc1α (Santa Cruz Biotechnology, Inc.), and SA1 and SA2 (Novus Biologicals). mAbs were obtained from the following sources: Flag (Sigma-Aldrich), Myc (EMD), HA (Sigma-Aldrich), Rad21 (Pati et al., 2002), and human CREST (provided by J. Craft, Yale University, New Haven, CT). All secondary antibodies for WBs were obtained from Rockland Immunochemicals. The following are sources of secondary antibodies for immunofluorescence: rhodamine-conjugated

anti–mouse IgG (Invitrogen) and FITC-conjugated donkey anti–goat, FITC-conjugated donkey anti–rabbit, and FITC-conjugated donkey anti–human IgG (Jackson ImmunoResearch Laboratories).

Plasmids

Full-length human cDNA encoding Rad21 (KIAA0078) and Smc1 (KIAA0178) were obtained from the Kazusa DNA Research Institute. Smc3 and SA2 cDNA were obtained from RZPD. SA1 and SA2 cDNA were provided by J.L. Barbero (Centro Nacional de Biotecnologia/Consejo Superior de Investigaciones Científicas, Madrid, Spain). Full-length human Rad21, Smc1, Smc3, SA1, and SA2 cDNAs were cloned into pCS2MT, pFlag CMV2, or pCruz HA mammalian expression vectors so that the tags are on the NT or CT of the cohesin proteins (Table S1, available at http://www.jcb.org/cgi/content/full/jcb.200801157/DC1).

Cell lines

HeLa and 293T cells were obtained from the American Type Culture Collection. Scc1-9×Myc HeLa Tet-On cell line was provided by J.-M. Peters (Research Institute of Molecular Pathology, Vienna, Austria).

Protein isolation

Cells were lysed with lysis buffer (in 10 ml containing 50 mM Tris-HCl, pH 7.4, 150 mM NaCl, 1 mM EDTA, 1% Triton X-100, 1 mM PMSF, one tablet of Complete protease inhibitor mix [Roche], and 100 µl phosphatase inhibitor cocktail sets I and II [Sigma-Aldrich]). The samples were incubated on ice for 10 min and centrifuged at 20,000 *g* at 4°C for 15 min. The supernatant was used for IP or SDS-PAGE.

To remove any possible nucleic acid contamination, we used EDTA-free lysis buffer to prepare the cell lysates. Before IP, the protein concentration was adjusted to 2 mg/ml. $MgCl_2$ was added to the final concentration of 0.4 mM. To 500 µg of cell lysates, we added 2.5 µl of 5 mg/ml DNase I and/or 0.5 µl of 10 mg/ml RNase A. The digestion was performed by rotating at RT for 10 min. EDTA was added to the final concentration of 5 mM to stop the nuclease activity before the cell lysate was used for IP.

IP

Rabbit anti–c-Myc pAb agarose (Sigma-Aldrich), monoclonal anti-Flag M2 affinity gel (Sigma-Aldrich), and monoclonal anti-HA agarose (Sigma-Aldrich) were used for IP. For each sample, 50 µl of 50% gel suspension and 1.5 mg of protein in 1,200 µl of lysis buffer were used. After rotation at 4°C for 3–4 h, the agarose gel was washed with 3 × 1 ml PBS, 1 × 0.5 ml of lysis buffer, and 1 × 1 ml PBS. The tagged proteins were eluted using respective peptide or 2 × SDS sample buffer.

IP of the endogenous cohesin subunits using antibodies was performed using the following protocol: cell lysate with 2 mg of protein in 1,200 µl of lysis buffer was precleared with 1 µg normal IgG plus 25 µl of 50% protein A– and G–conjugated agarose beads (EMD) at 4°C for 1 h. Next, 10 µg of primary antibody was added to the precleared cell lysate and rotated at 4°C for 2 h followed by adding 50 µl of 50% protein A– and G–conjugated agarose beads and rotating overnight. The agarose beads were washed, and the bound proteins were eluted with 120 µl of 2× SDS sample buffer.

Random primer PCR

Template DNA was isolated from cell lysates or elutes of IP using phenol/chloroform extraction. PCR was performed using the degenerated oligonucleotide primer PCR Master kit (Roche) and following the protocol provided by the manufacturer.

Fluorescent protein fragment complementation assay

pCDNA3.1/Zeo(+) vectors containing YFP(NT) and YFP(CT) were provided by S.W. Michnick (University of Montreal, Montreal, Canada). Full-length Rad21 cDNA was cloned into these vectors so that the YFP fragment is either at the NT or CT of Rad21. 293T and HeLa cells were cotransfected with constructs of YFP(NT)- and YFP(CT)-tagged Rad21. The fluorescence of YFP was examined 48 h after transfection using an inverted microscope (Axiovert 25; Carl Zeiss, Inc.) coupled to a high resolution digital camera (Axiocam; Carl Zeiss, Inc.) operated with Axiovision software (version 3.0; Carl Zeiss, Inc.). The images were taken using a 20 ×/0.3 or 40 ×/0.5 objective lens at RT.

siRNA

SA1 and SA2 siRNA (Thermo Fisher Scientific) were transfected using transfection reagent DharmaFECT 1 (Thermo Fisher Scientific). Silencer Negative Control #1 siRNA (Applied Biosystems) was used as a control. The transfection efficiency of siRNA was monitored using fluorescently labeled siGLO RISC-free siRNA (Thermo Fisher Scientific).

Immunofluorescence microscopy

Immunofluoresence microscopy was performed as described previously (Waizenegger et al., 2000). The samples were mounted using mounting medium (Vectashield; Vector Laboratories). Images were obtained with a microscope (E800; Nikon) equipped with Quips imaging software (Applied Imaging) and a 100×/1.4 objective lens (Nikon) at RT.

Yeast two hybrid

Rad21 wild-type (1–631 aa), NT-L (1–283 aa), CT-L (254–631 aa), and CT (451–631 aa)-truncated Rad21 cDNA were cloned in frame to fuse with Gal4-binding and -activating domains in pC97 and pC86 vectors, respectively. The yeast two-hybrid assay was performed as described previously (Pati et al., 1999).

Sucrose gradient centrifugation

Using Gradient Master (BioComp Instruments, Inc.), 5–30% of sucrose gradient was prepared. Cell lysate was overlaid to the top of sucrose gradient and centrifuged at 36,000 rpm for 16 h in an ultracentrifuge (L8-M; Beckman Coulter) with an SW-40 rotor. Using a Piston Gradient Fractionator (BioComp Instruments, Inc.), 0.25-ml fractions were taken. The protein in each fraction was precipitated using trichloroacetic acid. Cohesin proteins were detected with WBs and probed with the respective antibodies.

Online supplemental material

Table S1 shows all of the mammalian expression constructs used in this study and the strategy used for cloning the cohesin proteins. Fig. S1 shows the validation of epitope-tagged cohesin proteins using immunofluorescence microscopy, sucrose gradient centrifugation, and co-IP. Fig. S2 shows the co-IP of Flag-Rad21 and Myc-Rad21 in protein solution released from chromatin or whole cell lysate. Fig. S3 shows that Myc epitope tagging to the C-terminal but not the N-terminal Rad21 hinders Rad21–Rad21 interaction. Fig. S4 shows IP of YFP(NT)- and YFP(CT)-tagged Rad21. Fig. S5 shows immunofluorescence microscopy of Rad21 and Smc3 in SA1 and SA2 knockdown HeLa cells. Online supplemental material is available at http://www.jcb.org/cgi/content/full/jcb.200801157/DC1.

We thank Lisa Wang, James Huang, and Sharon Plon for critical reading of this manuscript.

This study was supported by Baylor College of Medicine startup funds and a grant from the National Cancer Institute (1RO1 CA109478) awarded to D. Pati.

Submitted: 24 January 2008
Accepted: 14 November 2008

References

Anderson, D.E., A. Losada, H.P. Erickson, and T. Hirano. 2002. Condensin and cohesin display different arm conformations with characteristic hinge angles. *J. Cell Biol.* 156:419–424.

Arumugam, P., S. Gruber, K. Tanaka, C.H. Haering, K. Mechtler, and K. Nasmyth. 2003. ATP hydrolysis is required for cohesin's association with chromosomes. *Curr. Biol.* 13:1941–1953.

Campbell, J.L., and O. Cohen-Fix. 2002. Chromosome cohesion: ring around the sisters? *Trends Biochem. Sci.* 27:492–495.

Chang, C.R., C.S. Wu, Y. Hom, and M.R. Gartenberg. 2005. Targeting of cohesin by transcriptionally silent chromatin. *Genes Dev.* 19:3031–3042.

Ciosk, R., W. Zachariae, C. Michaelis, A. Shevchenko, M. Mann, and K. Nasmyth. 1998. An ESP1/PDS1 complex regulates loss of sister chromatid cohesion at the metaphase to anaphase transition in yeast. *Cell.* 93:1067–1076.

Ciosk, R., M. Shirayama, A. Shevchenko, T. Tanaka, A. Toth, A. Shevchenko, and K. Nasmyth. 2000. Cohesin's binding to chromosomes depends on a separate complex consisting of Scc2 and Scc4 proteins. *Mol. Cell.* 5:243–254.

Cohen-Fix, O., J.M. Peters, M.W. Kirschner, and D. Koshland. 1996. Anaphase initiation in *Saccharomyces cerevisiae* is controlled by the APC-dependent degradation of the anaphase inhibitor Pds1p. *Genes Dev.* 10:3081–3093.

Darwiche, N., L.A. Freeman, and A. Strunnikov. 1999. Characterization of the components of the putative mammalian sister chromatid cohesion complex. *Gene.* 233:39–47.

Gause, M., H.A. Webber, Z. Misulovin, G. Haller, R.A. Rollins, J.C. Eissenberg, S.E. Bickel, and D. Dorsett. 2008. Functional links between *Drosophila* Nipped-B and cohesin in somatic and meiotic cells. *Chromosoma.* 117:51–66.

Gillespie, P.J., and T. Hirano. 2004. Scc2 couples replication licensing to sister chromatid cohesion in *Xenopus* egg extracts. *Curr. Biol.* 14:1598–1603.

Gimenez-Abian, J.F., I. Sumara, T. Hirota, S. Hauf, D. Gerlich, C. de la Torre, J. Ellenberg, and J.M. Peters. 2004. Regulation of sister chromatid cohesion between chromosome arms. *Curr. Biol.* 14:1187–1193.

Gruber, S., C.H. Haering, and K. Nasmyth. 2003. Chromosomal cohesin forms a ring. *Cell.* 112:765–777.

Gruber, S., P. Arumugam, Y. Katou, D. Kuglitsch, W. Helmhart, K. Shirahige, and K. Nasmyth. 2006. Evidence that loading of cohesin onto chromosomes involves opening of its SMC hinge. *Cell.* 127:523–537.

Guacci, V. 2007. Sister chromatid cohesion: the cohesin cleavage model does not ring true. *Genes Cells.* 12:693–708.

Guacci, V., D. Koshland, and A. Strunnikov. 1997. A direct link between sister chromatid cohesion and chromosome condensation revealed through the analysis of MCD1 in *S. cerevisiae*. *Cell.* 91:47–57.

Haering, C.H., and K. Nasmyth. 2003. Building and breaking bridges between sister chromatids. *Bioessays.* 25:1178–1191.

Haering, C.H., J. Lowe, A. Hochwagen, and K. Nasmyth. 2002. Molecular architecture of SMC proteins and the yeast cohesin complex. *Mol. Cell.* 9:773–788.

Hauf, S., I.C. Waizenegger, and J.M. Peters. 2001. Cohesin cleavage by separase required for anaphase and cytokinesis in human cells. *Science.* 293:1320–1323.

Hauf, S., E. Roitinger, B. Koch, C.M. Dittrich, K. Mechtler, and J.M. Peters. 2005. Dissociation of cohesin from chromosome arms and loss of arm cohesion during early mitosis depends on phosphorylation of SA2. *PLoS Biol.* 3:e69.

Huang, C.E., M. Milutinovich, and D. Koshland. 2005. Rings, bracelet or snaps: fashionable alternatives for Smc complexes. *Philos. Trans. R. Soc. Lond. B Biol. Sci.* 360:537–542.

Huang, J., and D. Moazed. 2006. Sister chromatid cohesion in silent chromatin: each sister to her own ring. *Genes Dev.* 20:132–137.

Ivanov, D., and K. Nasmyth. 2005. A topological interaction between cohesin rings and a circular minichromosome. *Cell.* 122:849–860.

Losada, A., and T. Hirano. 2005. Dynamic molecular linkers of the genome: the first decade of SMC proteins. *Genes Dev.* 19:1269–1287.

Losada, A., T. Yokochi, R. Kobayashi, and T. Hirano. 2000. Identification and characterization of SA/Scc3p subunits in the *Xenopus* and human cohesin complexes. *J. Cell Biol.* 150:405–416.

Mc Intyre, J., E.G. Muller, S. Weitzer, B.E. Snydsman, T.N. Davis, and F. Uhlmann. 2007. In vivo analysis of cohesin architecture using FRET in the budding yeast *Saccharomyces cerevisiae*. *EMBO J.* 26:3783–3793.

Michaelis, C., R. Ciosk, and K. Nasmyth. 1997. Cohesins: chromosomal proteins that prevent premature separation of sister chromatids. *Cell.* 91:35–45.

Michnick, S.W. 2003. Protein fragment complementation strategies for biochemical network mapping. *Curr. Opin. Biotechnol.* 14:610–617.

Milutinovich, M., and D.E. Koshland. 2003. Molecular biology. SMC complexes—wrapped up in controversy. *Science.* 300:1101–1102.

Misulovin, Z., Y.B. Schwartz, X.Y. Li, T.G. Kahn, M. Gause, S. MacArthur, J.C. Fay, M.B. Eisen, V. Pirrotta, M.D. Biggin, and D. Dorsett. 2008. Association of cohesin and Nipped-B with transcriptionally active regions of the *Drosophila melanogaster* genome. *Chromosoma.* 117:89–102.

Nakajima, M., K. Kumada, K. Hatakeyama, T. Noda, J.M. Peters, and T. Hirota. 2007. The complete removal of cohesin from chromosome arms depends on separase. *J. Cell Sci.* 120:4188–4196.

Nasmyth, K. 2005. How might cohesin hold sister chromatids together? *Philos. Trans. R. Soc. Lond. B Biol. Sci.* 360:483–496.

Pati, D., M.L. Meistrich, and S.E. Plon. 1999. Human Cdc34 and Rad6B ubiquitin-conjugating enzymes target repressors of cyclic AMP-induced transcription for proteolysis. *Mol. Cell. Biol.* 19:5001–5013.

Pati, D., N. Zhang, and S.E. Plon. 2002. Linking sister chromatid cohesion and apoptosis: role of Rad21. *Mol. Cell. Biol.* 22:8267–8277.

Remy, I., and S.W. Michnick. 2003. Dynamic visualization of expressed gene networks. *J. Cell. Physiol.* 196:419–429.

Skibbens, R.V. 2005. Unzipped and loaded: the role of DNA helicases and RFC clamp-loading complexes in sister chromatid cohesion. *J. Cell Biol.* 169:841–846.

Skibbens, R.V., M. Maradeo, and L. Eastman. 2007. Fork it over: the cohesion establishment factor Ctf7p and DNA replication. *J. Cell Sci.* 120:2471–2477.

Stead, K., C. Aguilar, T. Hartman, M. Drexel, P. Meluh, and V. Guacci. 2003. Pds5p regulates the maintenance of sister chromatid cohesion and is sumoylated to promote the dissolution of cohesion. *J. Cell Biol.* 163:729–741.

Strom, L., H.B. Lindroos, K. Shirahige, and C. Sjogren. 2004. Postreplicative recruitment of cohesin to double-strand breaks is required for DNA repair. *Mol. Cell.* 16:1003–1015.

Surcel, A., D. Koshland, H. Ma, and R.T. Simpson. 2008. Cohesin interaction with centromeric minichromosomes shows a multi-complex rod-shaped structure. *PLoS ONE.* 3:e2453.

Sumara, I., E. Vorlaufer, C. Gieffers, B.H. Peters, and J.M. Peters. 2000. Characterization of vertebrate cohesin complexes and their regulation in prophase. *J. Cell Biol.* 151:749–762.

Sumara, I., E. Vorlaufer, P.T. Stukenberg, O. Kelm, N. Redemann, E.A. Nigg, and J.M. Peters. 2002. The dissociation of cohesin from chromosomes in prophase is regulated by Polo-like kinase. *Mol. Cell.* 9:515–525.

Takahashi, T.S., P. Yiu, M.F. Chou, S. Gygi, and J.C. Walter. 2004. Recruitment of *Xenopus* Scc2 and cohesin to chromatin requires the pre-replication complex. *Nat. Cell Biol.* 6:991–996.

Uhlmann, F. 2004. The mechanism of sister chromatid cohesion. *Exp. Cell Res.* 296:80–85.

Unal, E., J.M. Heidinger-Pauli, and D. Koshland. 2007. DNA double-strand breaks trigger genome-wide sister-chromatid cohesion through Eco1 (Ctf7). *Science.* 317:245–248.

Waizenegger, I.C., S. Hauf, A. Meinke, and J.M. Peters. 2000. Two distinct pathways remove mammalian cohesin from chromosome arms in prophase and from centromeres in anaphase. *Cell.* 103:399–410.

Watrin, E., A. Schleiffer, K. Tanaka, F. Eisenhaber, K. Nasmyth, and J.M. Peters. 2006. Human Scc4 is required for cohesin binding to chromatin, sister-chromatid cohesion, and mitotic progression. *Curr. Biol.* 16:863–874.

Yeh, E., J. Haase, L.V. Paliulis, A. Joglekar, L. Bond, D. Bouck, E.D. Salmon, and K.S. Bloom. 2008. Pericentric chromatin is organized into an intramolecular loop in mitosis. *Curr. Biol.* 18:81–90.